
OVERCOMING 1 PART IN 10^9 OF EARTH ANGULAR ROTATION RATE MEASUREMENT WITH THE G WETTZELL DATA

A PREPRINT

A. D. V. Di Virgilio and G. Terreni
 INFN-Pisa largo B. Pontecorvo 3, 56127 Pisa, Italy
 angela.divirgilio@pi.infn.it

A. Basti, N. Beverini, G. Carelli, D. Ciampini, F. Fuso, E. Maccioni and P. Marsili
 Dep.of Physics Univ. of Pisa, largo B. Pontecorvo 3, 56127 Pisa, Italy

J. Kodet and K. U. Schreiber
 Technical University of Munich,
 FESG, Geodetic Observatory Wettzell,
 93444 Bad Kotzting, Germany

August 22, 2022

ABSTRACT

The absolute measurement of the Earth angular rotation rate with ground-based instruments becomes challenging if the 1 part in 10^9 of precision has to be obtained. This threshold is important for fundamental physics and for geodesy, to investigate effects of General Relativity and Lorentz violation in the gravity sector and to provide the fast variation of the Earth rotation rate. High sensitivity Ring Laser Gyroscopes (RLG) are currently the only promising technique to achieve this task in the near future, but their precision has been so far limited by systematics related to the laser operation. In this paper we analyze two different sets of observations, each of them three days long. They were obtained from the G ring laser at the Geodetic Observatory Wettzell. The applied method has been developed for the GINGERINO ring laser in order to identify and extract the laser systematics. For the available data sets the residuals show mostly white noise behavior and the Allan deviation drops below 1 part in 10^9 after an integration time of about 10^4 s.

1 Introduction

At present large scale ring laser gyroscopes (RLGs) are the most sensitive instruments to measure absolute angular rotation rates [1, 2, 3, 4, 5, 6]. They are based on high finesse square optical cavities where an active medium is present, and two counterpropagating laser beams are generated. The frequencies of the two beams depend on the effective time the photon takes to travel along the perimeter, which is different when the gyro is rotated. However, non-reciprocal effects in the cavity from the laser excitation process will cause a systematic bias and this has to be avoided.

Furthermore, there can be small deviations from the expected rate of rotation, due to fundamental laws of physics. One example is the precession of the frame of reference, as predicted by General Relativity (GR), related to gravitoelectric and gravitomagnetic effects.

For a RLG rigidly connected with the Earth surface, the observed Sagnac frequency is the difference in angular frequency of the two laser beams ω_s :

$$\omega_s = 8\pi \frac{A}{P\lambda} \Omega_{\oplus} \cos \theta, \quad (1)$$

where A is the area and P the perimeter of the ring cavity, λ the optical wavelength, Ω_{\oplus} the angular rotation rate, equivalent to the Earth rotation rate. θ is the angle between the optical cavity area vector and the Ω_{\oplus} rotation axis.

G has demonstrated a sensitivity of 12 prad/s in 1 s integration time and is able to operate continuously and unattended for months.[8] The sensitivity is a function of the size of the ring cavity and cavities of 77 and 121 m perimeter,[9] have been explored, several years ago. More recently the four component ring laser array ROMY has been installed in the geophysical observatory of Bavaria, Germany, which comprises 4 RLGs with triangular cavities, each with a perimeter of 36 m [2, 10]. Typically, the most sensitive existing devices capable of long term continuous operation employ square optical cavities with several meters on a side, rigidly attached to the ground. The mechanical structure of the optical cavity plays a big role in the performance of RLG and monolithic optical cavity structures have been the first RLGs to obtain relevant performance, getting close to tens prad/s level of sensitivity [1]. The G RLG, in operation at the Geodetic Observatory Wettzell, is the best known example and the optimal choice to have a very stable laser cavity. However, it is very difficult to build and cannot be reorientated easily. Over more than 20 years, heterolythic (HL) cavities have been developed, basically consisting of a rigid mounting frame giving hold to different mechanical elements, which support the mirrors contained inside metallic vacuum chambers.

GINGERINO has been the first HL RLG operating continuously with high sensitivity [11]. GINGERINO takes advantage of the quiet location inside the Gran Sasso, Italy, underground laboratory. Despite that, the standard deviation of the reconstructed Sagnac frequency of GINGERINO is typically more than 50 times larger than that of G [3, 4], mostly due to small mechanical issues, since the composed structure is not yet rigid enough[12]. Work is currently in progress to improve the mechanical HL design in order to increase the sensor stability. Despite these mechanical shortcomings in GINGERINO, the previous investigations [3, 4] indicate that the intrinsic noise level is lower than the expected shot noise limit for a RLG[13]. This model does not take the presence of the active medium inside the cavity into account and there is work in progress to improve the theoretical model by the Italian group of GINGER.

The main signal obtained from a RLG is the interferogram of the two counterpropagating beams transmitted at one corner of the square cavity. The Sagnac frequency ω_s , which is caused by the rate of rotation, must be not confused with the actually observed beat note ω_m of the interferogram [14, 15, 16, 17], since the latter is biased by laser systematics, usually caused by backscatter coupling and a null shift contribution. An original analysis scheme to remove laser systematics has been developed and successfully applied to analyse the data of GINGERINO [18, 19, 3, 4]. This effort shows how any change due to the laser dynamics can be approximated with the sum of several terms, analytically evaluated using the laser parameters of the Lamb theory. These in turn can be determined from the signals provided by the RLG. It is important to remark that these laser systematics are not a stochastic effect, since they are caused by all sorts of small changes affecting the active optical cavity. These effects are much smaller in monolithic RLGs.

2 Analysis procedure

The laser dynamics can be described by a set of differential equations containing several parameters, which are known as Lamb parameters [14, 15, 18, 19]. They can be calculated from the diagnostic signals, available from the ring laser intensities, in particular those providing the AC ($IS_{1,2}$) and the DC ($PH_{1,2}$) levels of the detectors, each looking at a different laser beam (hereafter denoted as monobeam signals) and their relative phase offset ϵ . The model refers to the intracavity power, while the signals are taken outside the cavity; it is therefore necessary to know the values of mirror transmission and detector gain.

The analysis proceeds in steps. The first approximation of the Sagnac frequency, denoted as ω_{s0} , is analytically evaluated as follows:

$$\omega_{s0} = \frac{1}{2} \sqrt{\frac{2IS_1IS_2\omega_m^2 \cos(2\epsilon)}{PH_1PH_2}} + \omega_m^2 + \frac{\omega_m}{2}, \quad (2)$$

where ω_m is the experimental interferometric angular frequency, that is the beat note of the interference of the two counterpropagating beams coming out from the cavity. It must be noted that the monobeam intensities enter Eq. 2 as the ratio of their AC and DC components, leading to mirror transmission and the differences in electronic gains to play a smaller role. For many applications, ω_{s0} is indeed a good approximation of ω_s .

Nevertheless, the different terms of the equation are certainly affected by errors, as for example the dark current of the applied photodiodes or any non-linearity in the electronic gain. In order to improve the ω_{s0} evaluation, six terms, namely ω_{ξ} , have been elaborated, assuming small errors in the measurement data used in Eq. 2 and expanding the equation to the first order. The first term was already discussed in the first paper dedicated to the analysis method [18], the other ones have been added more recently. We remark that the six ω_{ξ} terms do not depend on the laser dynamics and are meant to improve ω_{s0} by correcting errors associated with the measurements themselves.

The null shift depends on the Lamb parameters associated with the laser excitation and is obtained by the term ω_{ns1} , the first order expansion of the theory. Higher order expansion terms can be calculated, but in the following analysis only the first one will be used. The null shift is strictly connected to the non-reciprocity of the optical path in the two directions, related in turn to dissipative processes. In terms of the Lamb parameters of the laser functions, ω_{ns1} is connected to the difference $\mu_c - \mu_{cc}$ between the cavity losses, where $\mu_{c,cc}$ represent losses in clockwise and counter-clockwise propagation directions. However, it has been demonstrated in [18] that, assuming a quasi-stationary laser and the same value for the parameter β for the two beams¹, the loss difference is made explicit, so that only one of the two $\mu_{c,cc}$ is a free parameter. In the following, we will consider only the clockwise cavity loss, which will be indicated simply as μ ; ω_{ns1} and β are proportional to μ and completely defined by the theory in terms of the available signals. The null shift correction has values in the region of mHz (several ppm), so the accuracy of μ , usually measured by the ring-down time of the optical cavity with percent accuracy, can severely limit the ω_s reconstruction. The analysis developed for GINGERINO assumes constant the plasma temperature and pressure, while μ changes with time, accordingly any change is interpreted as change of μ , but it could be due to the other parameters, or to the electronic circuit regulating the gain tube. In the future the analysis model will be further expanded in order to better identify the origin of the changes. A suitable procedure is developed to take into account variations of μ with time and refine the identification of the null shift. Changes of μ in time, however, are small and slow enough to not invalidate the assumption of a quasi-stationary regime. It is possible to consider $\mu(t) = \mu(t_0) + \delta\mu(t)$, t_0 being the origin of the expansion in the series. It is convenient to describe $\delta\mu(t)$ using the available signals. To this aim, the laser gain monitor signal can be used, but in more recent versions of the analysis the Lamb parameter β has been considered, since it is rather constant in time and proportional to μ . By using the relationship reported in the appendix of [19] and the parameters of the RLG G, we have

$$\beta = \frac{2.98772\mu}{2.98772 - PH_1}, \quad (3)$$

where PH_1 is the DC value of monobeam 1, in Volts. Equation 3 shows that μ is a proportionality constant, accordingly the quantity that can be evaluated does not contain μ . Assuming $\mu(t) = \mu(t_0) + \delta\mu(t)$, and taking into account that β is rather constant, since it is related to the laser transition, $\delta\mu(t)$ can be evaluated at the first approximation as follows:

$$\begin{aligned} \bar{\beta} &= \frac{\beta(t)}{\mu} \\ \delta\mu(t) &= \mu(t_0) \times \left(\frac{\bar{\beta}(t_0)}{\bar{\beta}(t)} - 1 \right). \end{aligned} \quad (4)$$

In this way, $\mu(t_0)$, the loss at the time t_0 , has to be determined by statistical means, with t_0 arbitrarily chosen: in the present analysis t_0 is the central point of the data set. The Lamb parameters can be considered constant over short time intervals; therefore, the stationary mathematical relationships can be considered valid for short time intervals. Accordingly the required analytical relationships are elaborated at high frequency rate, and decimated afterwards down to the desired low frequency rate, details can be found in the related literature[18, 19].

The second step of the analysis determines ω_s with a linear regression to optimize the subtraction of the ω_ξ terms, ω_{ns1} and $\omega_{ns1} \times \delta\mu$. In this way, ω_s is recovered, but it is still necessary to further identify and subtract other known signals. The G RLG is well isolated, but in any case affected by global and local motion of the Earth crust, such as the diurnal polar motion and the solid Earth tides. In the present analysis the direct effect of the environmental disturbances on the mechanical apparatus is considered negligible, owing to the monolithic and stable ZERODUR² structure. It is assumed that all external effects, hereafter denoted geodetic components, can be described by sufficiently accurate models. The geodetic components are well known, but they are added to the linear regression along with the other terms in order to avoid biases induced by previous analyses. The terms relevant to describe the main geodetic components are taken from model data provided by the G group. Furthermore, it is also possible to take the angular rotation around the vertical in the local reference frame at the G latitude and longitude into account. They are based on the publications of the International Earth Rotation and Reference Systems Service (IERS)³ We denote relevant terms as *FGEO*. It is important to remark that *FGEO* contains the Chandler and the Annual wobble, whose values are published with several days delay. For this reason these signals are not included in the near realtime data files of G. Finally, we have verified that the calibration and alignment of G is at the level of 0.3%.

¹ $\beta_{1,2}$ is the self-saturation parameter of the laser transition for the two counter-propagating beams. In the model it is assumed $\beta_c = \beta_{cc} = \beta$.

²ZERODUR is a glass with very low thermal expansion coefficient, that can be considered practically negligible at room temperature.

³<https://hpiers.obspm.fr/eop-pc/index.php?index=C04&lang=en>.

Gas pressure	10 mbar
Area of the beam at waist	$0.51 \times 0.74^{-6} \text{ m}^2$
Mirror transmission	0.2 ppm
Perimeter of the cavity	16 m
Kinetic discharge temperature	360 K
Photodiode quantum efficiency	0.5
Trans-impedance amplifier gain	$1.1 \times 10^8 \text{ V/A}$
Beat note mean value	348.516 Hz
average loss $\langle \mu \rangle$	6.51280×10^{-5}
Scale factor	$6.3211125158 \times 10^6 \text{ Hz s/rad}$

Table 1: Data of the G RLG set up.

2.1 Details of data analysis

The whole analysis is based on linear regression (LR) [20, 21, 22, 23]. Only terms with p-values below 0.4 are kept in the linear regression, carried out by using the MATLAB routine *fitlm*, with the option *RobustOpt* on. It has been checked that the final p-values are always below 0.2. The reconstruction of the AC and DC signals is based on Hilbert transform: data are band-pass filtered around the beat note (in a range ± 12 Hz around ω_m) and Blackman windowing is implemented. This part of the analysis has been validated by processing a known ideal sinusoidal signal, without noise addition. It has been checked that the Hilbert transform routine leads to recover the expected frequency within 7 nHz before decimation, and within 5 nHz after decimation down to the rate of 0.016667 Hz (60 s measurement time). Relevant terms in the analysis are evaluated at 2 kHz, the rate of the available data, and decimated down to 0.016667 Hz rate, taking into account the information provided by the G group.

A set of explanatory variables is evaluated: the laser explanatory variables ω_ξ , ω_{ns1} , $\omega_{ns1} \times \delta\mu$, and the available geodetic terms. The LR procedure has been repeated using different schemes. In the first scheme the LR uses the whole set of terms all at once. In the second scheme the LR has been applied in two steps: the first step evaluates ω_s using only the laser terms, leading to an initial evaluation of the laser corrections. In the second step the geodetic terms are used as explanatory variables. When available, *FGEO* is added as a known signal and used for check. The different schemes produce always very similar results: in the following, the first scheme is used, since it is the more conservative one. Care has been put to avoid local minima in the regression, which sometimes occurred.

2.2 The data

The two data sets have 3 full days stored at 2 kHz rate, day 99, 100, and 101, year 2020, and day 121, 122, and 123, year 2022. The two data sets are different and the 2020 one presents more short duration glitches than the other. The G data, all the related analysis steps, the employed geophysical models, and environmental monitors are stored on a daily basis in a file at 0.016667 Hz rate. Details of data associated to each column of the published files can be found in the Appendix: in the following, the column numbers will be used in the analysis description. Column 34 provides the measured Earth rotation with the the estimated backscatter correction applied and the theoretical diurnal polar motion and solid Earth tides model subtracted. Since the absolute orientation of the G structure is not known well enough, these latter corrections have to be considered as preliminary. Several tiltmeters are used in order to establish the long term changes of the sensor orientation. These in turn have to be corrected for temperature related effects and from mass attraction derived from a global weather model [7]. In particular the latter comes with several days delay, hence it can not be corrected in realtime. The initial value of the ring laser orientation is taken from a local survey, which provides values with a substantial error, much larger than 5 ppm. Typical values are 49.144802 degrees for the latitude and 12.87630 degrees for the longitude. While the analysis is based on the methods developed for GINGERINO, there are several differences in the experimental readout system. In GINGERINO the interferogram is the beat note taken at one corner and the monobeams are both measured at the same neighboring corner. For G, the available interferogram is the sum of the two beams at the beam combiner, and the monobeams are each measured at a different corner in order to avoid perturbations from back reflections. In this case the ω_ξ terms are effective in correcting differences in the mirror transmission, and other differences due to the measurement at different corners.

3 Analysis results

The beat note ω_m is evaluated with our method and compared with the one recorded in the published file, contained in column 3.

There are small differences in the standard deviation, which in the present analysis turns out smaller by $3 - 4 \mu\text{Hz}$, probably due to the band-pass filter around the beat note applied before the frequency reconstruction. This is relevant to reduce the impact of the laser systematic terms ω_{K1} and ω_{K2} [18, 19], first and second order expansion, since the second harmonic contribution, which is very difficult to model and subtract, is effectively eliminated in this way.

Remarkably, in the present data sets irregular signals occur in the separation between one and the subsequent day, in fact to keep constant the number of data for each day some points are missing at the end of each daily file, standard procedure of the Minisced data retrieval. In the analysis the missing points are replaced with zeroes.

3.1 Days 99-101, 2020

We have analysed the days 99, 100 and 101 starting from raw data. Published files, containing one day data, are extracted from a continuous logging sequence with the help of a MINISEED data format, and, to prevent loss of precision, a set of data in a MATLAB readable format has been used. Analogously to the procedure used for GINGERINO, data are band-passed around $\omega_m = 348 \text{ Hz}$, in a $\pm 12 \text{ Hz}$ interval. The relevant parameters are evaluated (AC and DC of the monobeams, relative phase of the mode ϵ , and the beat note ω_m) at 2 kHz rate. Different terms of the analysis, ω_{s0} , ω_ξ , and ω_{ns1} are evaluated using the available information summarized in Table 1, including photodiode gain, parameters of the G RLG (size and gas pressure), the measured average losses $\langle \mu \rangle$. Six ω_ξ terms are considered, to take into account errors in the evaluation of ϵ , $I_{S1,2}$, and $PH_{1,2}$ of the monobeams.

The first step of the analysis evaluates ω_{s0} using Eq. 2. Remarkably, ω_{s0} values remain rather stable within each single day, but small discontinuities are evident between one day and the other, due to the fact that some points around midnight are missing.

For this reason data around midnight have been eliminated from the analysis: no other cuts have been applied to the data.

Figure 1 shows ω_s , mean value subtracted, evaluated by the LR procedure for the three days (red solid line), and the discontinuities between different days are no longer evident. ω_m , mean values subtracted, is also shown (blue solid line): small differences with ω_s are seen.

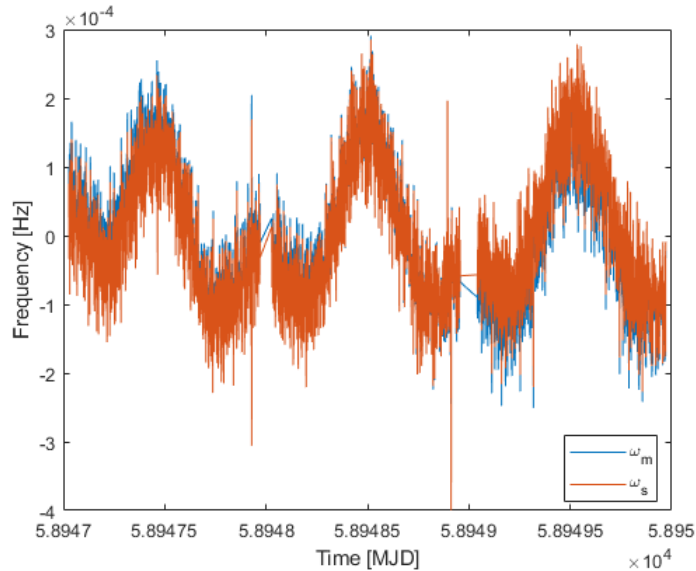


Figure 1: Comparison of ω_s (red) and ω_m (blue) evaluated on the 2020 three days data set: mean values are subtracted in both cases. The 2020 three days data set is considered

The top panel of Fig. 2 reports the ω_{ns1} corrections evaluated by the LR procedure. The total geodetic components are plotted in the bottom panel, as evaluated by the LR procedure without including Chandler wobble data.

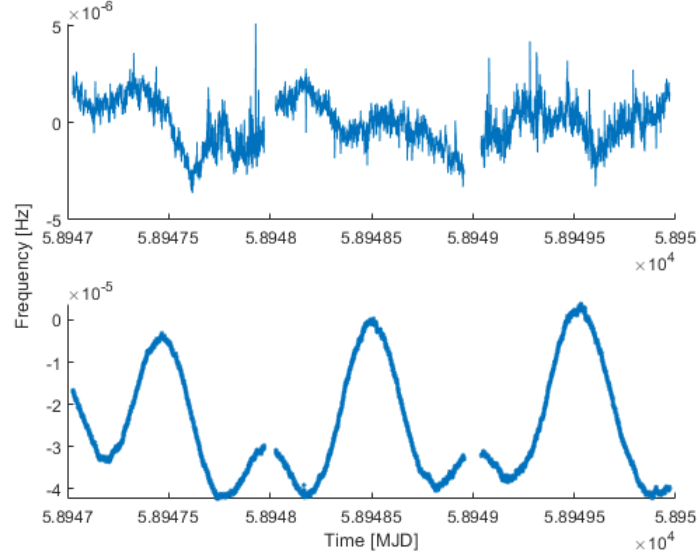


Figure 2: Sum of the laser terms (top), total geodetic components as evaluated by the procedure (bottom), without including Chandler wobble data. The 2020 three days data set is considered.

3.2 Days 121-123, 2022

A second, more recent, set of three days (day 121, 122, and 123, year 2022) has been also analysed. In this second data set the G RLG was operating under ideal conditions and at roughly 20% lower beam power. The signals are cleaner, although small discontinuities between different days are still present, but fewer points have been eliminated around midnight to cure the problem. The ω_s has been evaluated analogously to the first data set. Data indicate that the signal is more stable compared with the previous set of data, accordingly the null shift terms have little impact, but remain to be meaningful for the Allan deviation analysis. Figure 3 and Fig. 1 are very similar with each other.

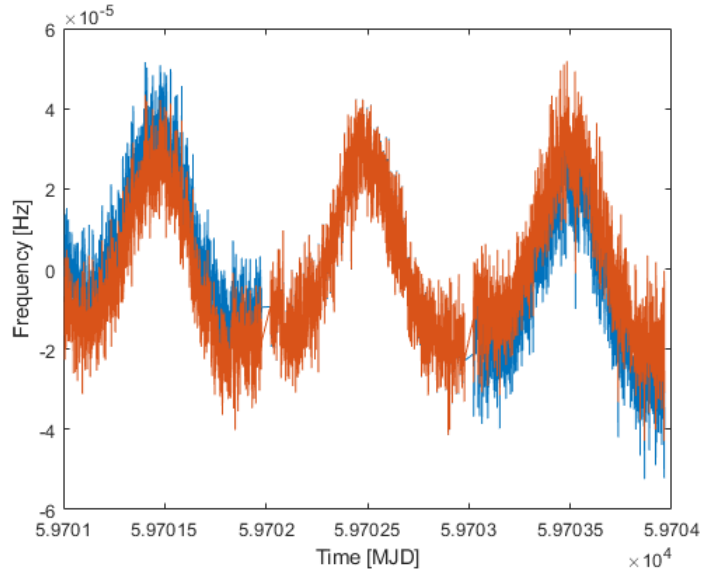


Figure 3: Same of Fig. 1 for the 2022 three days data set.

4 Residuals and Allan deviation of the two data sets

The two data sets exhibit very similar results, however, more points have been eliminated in the 2020 case, probably in response to the higher beam power setting. The amount of data retained for the analysis is 93.4% of the total for the 2020 and 95.8% of the total for the 2022 data set. All cuts had to be applied around midnight. Figure 4 shows the distributions of the residuals for both sets; they are very similar with respect to each other. This indicates that the noise from the laser dynamics has been effectively identified and subtracted by the procedure in both cases.

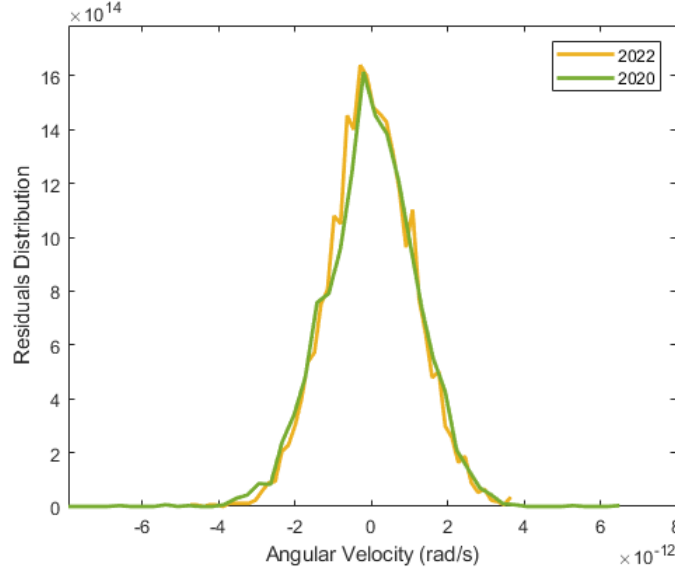


Figure 4: Distribution of the residuals for the two data sets expressed as angular velocity. The standard deviations are $7.73 \pm 0.05 \mu\text{Hz}$ and $7.14 \pm 0.05 \mu\text{Hz}$ for the 2020 and 2022 data sets, respectively.

Figure 5 shows the Allan⁴ deviation of the residuals for both data sets, sampled at 0.016667 Hz. The green solid lines display results obtained by applying the LR procedure at once on the whole three days data sets. The procedure has been also applied to each single day separately: orange solid lines report the corresponding results (day 99, year 2020, and day 121, year 2022, are considered as examples). Remarkably, plots cross the 1 part in 10^9 threshold in less than one day of integration time, albeit with a larger standard deviation.

The same procedure has been applied to each single day separately and the two panels in Fig. 5 refer to the Allan deviation of the residuals. Curves obtained in the present analysis are always below those coming out from the standard one, with the exception of one of the days, around $\tau \simeq 8 \times 10^3$ s. When *FGEO* contributions are taken into account, the present analysis leads to even smaller Allan deviation. In any case, plots cross the 1 part in 10^9 threshold with less than 1 day of integration time.

At the present stage we do not investigate the nature of the residuals, since the focus is here to investigate whether the Allan deviation goes below the fundamental physics threshold, i.e., below about 1 part in 10^9 , while keeping the analysis as simple as possible. Moreover, owing to its monolithic structure, G is certainly less prone to those mechanical coupling effects accounted for, in GINGERINO analysis, by the extra term based on the product of the residuals and the tiltmeter signal.

The geophysical components have been subtracted to ω_m using the LR, without taking into account the laser terms ω_ξ and ω_{ns1} . With the 2022 data set, definitely less affected by laser dynamics, the Allan deviation is a factor 2 worse at 10^4 seconds compared to Fig. 5 RIGHT, where the Allan shown with the dashed red line is super-imposed. With the 2020 data set, the result is even higher, indicating that, despite G is based on an extremely rigid optical cavity, it is necessary to identify and subtract the laser systematic terms in order to reach, and go beyond, the 1 part in 10^9 precision level of the Earth rotation rate measurement.

⁴The function `allan` of Matlab has been used.

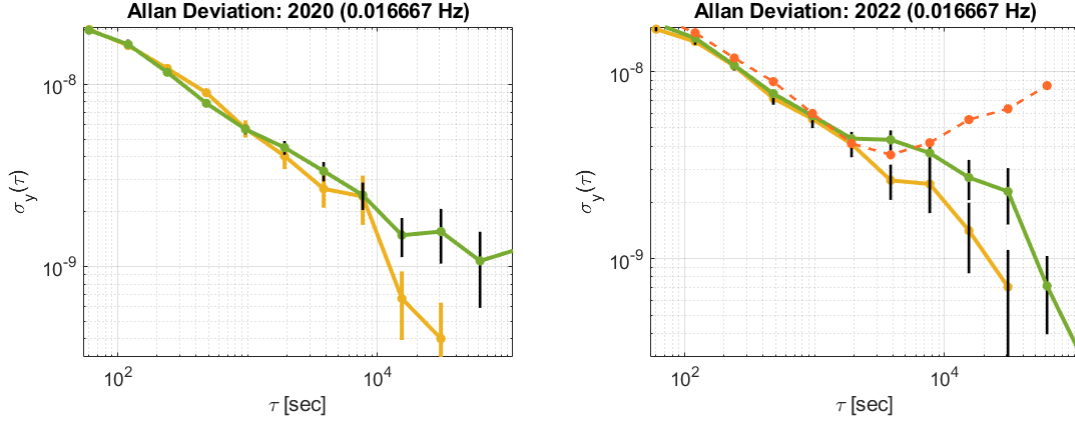


Figure 5: LEFT: 2020, Allan deviation obtained according to the available analyses, for the 3 days (green) and day 99 (orange). RIGHT: 2022, Allan deviation obtained according to the available analyses, for the 3 days (green) and day 121 (orange). The red dashed line in the right figure shows the Allan deviation subtracting only the geophysical components from the beat note ω_m .

5 Conclusions

The analysis based on the model developed for GINGERINO has been extended to the G RLG, rewriting the mathematical relationships with the main aim to account for the characteristic values of the G apparatus. In this way, corrections to the laser systematics have been subtracted in a deterministic way following the model based on the stationary solution of the RLG equations and the loss $\bar{\mu}$ of the optical cavity determined by statistical means. The signals of geodetic origin have been always subtracted assuming linear relationships to minimize the residuals via linear regression. For the full set of three days of 2020, the Allan deviation drops below one part in 10^9 in less than 1 day of integration time.

The data point close to midnight are eliminated, to overcome a problem in the data retrieval subroutine and the separate analysis of each single day exhibits Allan deviations going below 1 part in 10^9 more rapidly.

The analysis has been repeated with a second, and more recent, set of three days in June 2022, where the ring laser was operated at lower power. In this case, the monobeam signals are cleaner, and the cavity appears to be more stable, accordingly the effects of ω_{ns1} are smaller, but still remain significant for the lower Allan deviation outcome.

G is based on a monolithic structure in ZERODUR, a very low thermal expansion material, with mirrors optically contacted to the structure. For this reason the cavity is extremely stable, nevertheless tiny laser systematic effects are present and it is necessary to subtract them in order to improve the performance above the 1 part in 10^9 level. Certainly laser systematics cancellation is more relevant for RLGs based on a HL design, as GINGERINO and ROMY, since in this case cavity losses, the quantity effectively ruling laser systematics, is affected by variations of the mirror distances and their relative alignment.

References

- [1] K. U. Schreiber and K.U. Wells, *Large ring lasers for rotation sensing*, Rev. Scient. Instr. 84, 041101 (2013).
- [2] Heiner Igel *et al.* ROMY: a multicomponent ring laser for geodesy and geophysics, Geophysical Journal International, Volume 225, Issue 1, April 2021, Pages 684-698.
- [3] Angela D. V. Di Virgilio *et al.* Underground Sagnac gyroscope with sub-prad/s rotation rate sensitivity Phys. Rev. Research 2, 032069(R) (2020).
- [4] A. D. V. Di Virgilio *et al.*, Sensitivity limit investigation of a Sagnac gyroscope through linear regression analysis Eur. Phys. J. C, 81, 400 (2021).
- [5] D. Zou *et al.*, Gyroscopic performance and some seismic measurements made with a 10 meter perimeter ring laser gyro, Appl. Opt. 60, 1737-1743 (2021).
- [6] K. Liu *et al.*, Large-scale passive laser gyroscope for earth rotation sensing, Optics Letters, 44, 11, 2732-2735 (2019).

- [7] Klügel, T., Wziontek, H. *Correcting gravimeters and tiltmeters for atmospheric mass attraction using operational weather models*, Journal of Geodynamics 48, 204–210 (2009).
- [8] K. U. Schreiber, T. Klügel, J.-P. R. Wells, R. B. Hurst, and A. Gebauer, *How to detect the Chandler and the annual wobble of the Earth with a large ring laser gyroscope*, Phys. Rev. Lett. 107, 173904 (2011).
- [9] Robert W. Dunn, Dmitry E. Shabalin, Robert J. Thirkettle, *et al.*, *Design and initial operation of a 367-m2 rectangular ring laser* Vol. 41, APPLIED OPTICS 1685, (2002).
- [10] A. Gebauer *et al.* *Reconstruction of the Instantaneous Earth Rotation Vector with Sub -Arcsecond Resolution Using a Large Scale Ring Laser Array* Phys. Rev. Lett. 125, 033605 (2020)
- [11] J. Belfi, N. Beverini, G. Carelli, A. Di Virgilio, U. Giacomelli, E. Maccioni, A. Simonelli, F. Stefani, and G. Terreni, *Analysis of 90 day operation of the GINGERINO gyroscope*, Appl. Opt. 57, 5844-5851 (2018)
- [12] Basti, A., Beverini, N., Bosi, F. *et al.*, *Effects of temperature variations in high-sensitivity Sagnac gyroscope*, Eur. Phys. J. Plus 136, 537 (2021).
- [13] W. Chow *et al.*, *The ring laser gyro*, Rev. Mod. Phys. 57.61 (1985).
- [14] L. N. Menegozzi and W. E. Lamb. *Theory of a ring laser*, Phys. Rev. A, **8**:4, (1973).
- [15] F. Aronowitz and R. J. Collins. *Lock-in and intensity-phase interaction in the ring laser*,. Journal of Applied Physics, **41**:1, (1970).
- [16] A. Beghi, *et al.*. *Compensation of the laser parameter fluctuations in large ring-laser gyros: a kalman filter approach*. Appl. Opt., **51**(31):7518-7528, (2012).
- [17] D. Cuccato, A. Beghi, J. Belfi, N. Beverini, A. Ortolan, and A. Di Virgilio. *Controlling the nonlinear inter cavity dynamics of large he-ne laser gyroscopes*. Metrologia, **51**:97-107, (2014).
- [18] A. D. V. Di Virgilio, N. Beverini, G. Carelli, D. Ciampini, F. Fuso, and E. Maccioni, Eur. Phys. J. C **79**, 573 (2019).
- [19] A. D. V. Di Virgilio, N. Beverini, *et al.*, Eur. Phys. J. C **80**, 163 (2020).
- [20] Kay, Steven M., *Fundamentals of Statistical Signal Processing: Estimation Theory*, Prentice-Hall, Inc., US, (1993).
- [21] J. Neter, M. H. Kutner, C. J. Nachtsheim, and W. Wasserman, *Applied Linear Statistical Models*, Irwin, Chicago (1996).
- [22] A. Sen and M. Srivastava. *Regression Analysis: Theory, Methods, and Applications*, Springer Texts in Statistics. Springer New York (1997).
- [23] F. Di Renzo, *Characterisation and mitigation of non-stationary noise in Advance Gravitational Wave Detectors*, PhD Thesis in Physics, University of Pisa, **etd-06192020-081853** , June 2020.

A The G daily file with data and results

On a daily basis, G data sampled at 0.0166667 Hz rate and relevant results are published in a file. Contents of each column are listed in Table 2.

Column	Quantity	Units
1	Epoch	[MJD]
2	Epoch	[day]
3	Sagnac (single tone extractor)	[Hz]
4	Sagnac rms	[Hz]
5	Phase between SW-port and Sagnac beam combiner port	[rad]
6	Phase between SE-port and Sagnac beam combiner port	[rad]
7	SW-AC	[V]
8	SW-DC	[V]
9	SW-AC/DC	-
10	SE-AC	[V]
11	SE-DC	[V]
12	SE-AC/DC	-
13	SW-SE-Phase	[rad]
14	estimated Sagnac correction factor	-
15	estimated Sagnac correction value	[mHz]
16	Sagnac BS-corrected	[Hz]
17	SE-DDS-Amplitude AC-level for driving LED	[V]
18	SW-DDS-Amplitude AC-level for driving LED	[V]
19	SW-Phase to DDS driving LED	[rad]
20	SE-Phase to DDS driving LED	[rad]
21	Sagnac geophys. model contribution subtracted (Oppolzer-Terms & Tilt-NS deformation effect)	[Hz]
22	Sagnac of SE-monobeam estimation (Single Tone extractor)	[Hz]
23	Sagnac of SW-monobeam estimation (Single Tone extractor)	[Hz]
24	Geophysical Model: Oppolzer terms NS	[rad]
25	Geophysical Model: Oppolzer terms EW	[rad]
26	Geophysical Model: Theoretical tilt NS (attraction part)	[rad]
27	Geophysical Model: Theoretical tilt NS (deformation part)	[rad]
28	Observed tilt NS	[rad]
29	Geophysical Model: Theoretical tilt EW (attraction part)	[rad]
30	Geophysical Model: Theoretical tilt EW (deformation part)	[rad]
31	Observed tilt EW	[rad]
32	Geophysical Model: Sagnac geophys. model contribution (Oppolzer-Terms & Tilt-NS deformation effect)	[μ Hz]
33	Sagnac geophys. model reduced (Oppolzer-Terms & Tilt-NS deformation effect)	[Hz]
34	Sagnac geophys. model and BS applied	[Hz]
35	Pressure vessel barometric pressure (Paroscientific at pressure vessel supply)	[hPa]
36	Pressure vessel temperature	[$^{\circ}$ C]
37	Pressure vessel humidity	[%rH]
38	Ringlaser room barometric pressure (Vaisala outside pressure vessel)	[hPa]
39	Ringlaser room temperature	[$^{\circ}$ C]
40	Ringlaser room humidity	[%rH]
41	Control room temperature	[$^{\circ}$ C]
42	Control room humidity	[%rH]
43	Plasma brightness	[V]

Table 2: Content of columns in the G data and results file.